

CONTROL OF SPINTRONIC AND ELECTRONIC PROPERTIES OF BIMETALLIC AND VACANCY-ORDERED VANADIUM CARBIDE MXENES VIA SURFACE FUNCTIONALIZATION

A PREPRINT

Shuo Li

Department of Physical and Macromolecular Chemistry, Faculty of Science
Charles University in Prague, 128 43 Prague 2, Czech Republic
lishu@natur.cuni.cz

Junjie He

Bremen Center for Computational Materials Science
University of Bremen, Am Fallturm 1, 28359 Bremen, Germany

Petr Nachtigall

Department of Physical and Macromolecular Chemistry, Faculty of Science
Charles University in Prague, 128 43 Prague 2, Czech Republic

Lukáš Grajciar

Department of Physical and Macromolecular Chemistry, Faculty of Science
Charles University in Prague, 128 43 Prague 2, Czech Republic

Federico Brivio *

Department of Physical and Macromolecular Chemistry, Faculty of Science
Charles University in Prague, 128 43 Prague 2, Czech Republic
briviof@natur.cuni.cz

September 7, 2021

ABSTRACT

MXenes are 2D transition metal carbides with high potential for overcoming limitations of conventional two-dimensional electronics. In this context, various MXenes have shown magnetic properties suitable for applications in spintronics, yet the number of MXenes reported so far is far smaller than their parental MAX phases. Therefore, we have studied the structural, electronic and magnetic properties of bimetallic and vacancy-ordered MXenes derived from a new $(V_{2/3}Zr_{1/3})_2AlC$ MAX phase to assess whether MXene exfoliation would return stable magnetic materials. In particular, we have investigated the properties of pristine and surface-functionalized $(V_{2/3}Zr_{1/3})_2CX_2$ bimetallic and $(V_{2/3}\square_{1/3})_2CX_2$ vacancy-ordered MXenes with $X = O, F$ and OH . Our density functional theory (DFT) calculations showed that modifying the MXene stoichiometry and/or MXene surface functionalization changes MXene properties. After testing all possible combinations of metallic motifs and functionalization, we identified $(V_{2/3}Zr_{1/3})_2CX_2$, $(V_{2/3}\square_{1/3})_2CF_2$ and $(V_{2/3}\square_{1/3})_2C(OH)_2$ as stable structures. Among them, $(V_{2/3}Zr_{1/3})_2CO_2$ MXene is predicted to be an FM intrinsic half-semiconductor with a remarkably high Curie temperature (T_C) of 270 K. The $(V_{2/3}Zr_{1/3})_2C(OH)_2$ MXene exhibits a rather low work function (WF) (1.37 eV) and is thus a promising candidate for ultra-low work function electron emitters. Conversely, the $(V_{2/3}\square_{1/3})_2CF_2$ MXene has a rather high WF and hence can be used as a hole injector for Schottky-barrier-free contact applications. Overall,

our proof-of-concept study shows that theoretical predictions of MXene exfoliation and properties support further experimental research towards developing spintronics devices.

Keywords MXene · functionalization · Spintronics

1 Introduction

2D materials are currently the subject of intense experimental and theoretical research for their extremely high aspect ratio, which accounts for their remarkable electronic and magnetic properties. Since graphene[1] was first isolated, several other ultrathin 2D materials with the same honeycomb lattice have been described, such as boron nitride (h-BN)[2], silicene[3], transition metal dichalcogenides[4, 5], monolayer black phosphorus[6] and MXenes[7], among others[8]. MXenes are particularly appealing as candidates for spintronics, i.e., the manipulation of electronic spin for logic devices[9]. However, the magnetic response required for spintronics applications is relatively rare in 2D materials[10]. While magnetism can be introduced in various ways, e.g., via defects or dopants engineering or with external electric fields, our ability to control operational parameters for practical devices remains limited [11]. For example, although phases with high spin-polarization can be achieved in transition metal dichalcogenides, controlling the distribution of dopants and defects is highly difficult [12, 13, 14]. Accordingly, the design of new intrinsic 2D magnetic materials (which would not require such complicated engineering) would greatly improve their potential for spintronics applications. Several such new classes of compounds have emerged in recent years[15, 16], including: half-metals[14, 17, 18], spin gapless semiconductors[19, 20], bipolar magnetic semiconductors[21] and half-semiconductors[22, 23, 24]. Among them, half-semiconductors and half-metals have shown the most promising results regarding spin generation, injection, storage and detection [25, 26], thus paving the way forward towards a new type of computer components.

MXenes are 2D transition metal carbides (or nitrides) with the general formula M_2C (where M is a transitional metal) derived from the corresponding MAX phase structures by exfoliation upon chemical etching in aqueous hydrofluoric acid at room temperature[27, 28]. As a result of their synthesis, MXene surfaces are typically functionalized with surface-terminating groups such as O, F or OH[7]. Considering their properties, MXenes have been proposed as materials suitable for applications such as transparent conductive films, electromagnetic interference absorption and shielding devices, electrocatalysts, lithium-ion batteries cathodes and supercapacitors[29, 30, 31]. In particular, many MXenes have shown potential for spintronics since they are often half semiconductors or half metals[14, 17, 18]. In the first case, the conduction band minimum (CBM) and the valence band maximum (VBM) are both fully polarized and both spin channels show a band gap. Conversely, only one channel shows a band gap, while the other is metallic in half metals. Several MXenes have also been predicted to be either half semiconductors or half metals, albeit with limited experimental evidence[14, 17, 18, 32]. Moreover, the electronic structures of MXenes can be fine-tuned by surface modification[33, 34]. Therefore, MXenes are candidates for other applications[35, 36], such as emitter cathodes in light emitting diodes and field effect transistors[37, 38].

The development of MAX phases with bimetallic composition, in particular $(Mo_{2/3}Sc_{1/3})_2AlC$ [39, 40, 41] and $(V_{2/3}Zr_{1/3})_2AlC$ [42], has recently opened new MXene research avenues. These bimetallic MXenes (often denoted metal-doped) with functionalized surfaces can be exfoliated by precisely controlling the thermodynamic conditions [39, 40]. In addition, a vacancy-ordered MXene $(Mo_{2/3}\square_{1/3})_2C$ (where \square denotes the missing transition metal atom) has been reported. Using first-principles calculations, H. Lind *et al.*[43] have computationally shown how introducing different surface functional groups can be used to tune the band gap of $(Mo_{2/3}\square_{1/3})_2C$. In this context, we computationally investigated the MAX phase $(V_{2/3}Zr_{1/3})_2AlC$ and the properties of the corresponding bimetallic $(V_{2/3}Zr_{1/3})_2C$ MXene and related vacancy-ordered $(V_{2/3}\square_{1/3})_2C$ MXene. Our aim is to determine whether suitable surface functionalization affects the electronic and magnetic properties of both $(V_{2/3}Zr_{1/3})_2CX_2$ and $(V_{2/3}\square_{1/3})_2CX_2$ ($X = O, F$ and OH) MXenes based on first-principles calculations.

2 Methods

Density functional theory (DFT) was used to identify structures and electronic and magnetic properties of MXenes along with the *ab-initio* molecular dynamics (AIMD) and Monte Carlo methods for calculating the kinetic stability and Curie temperature of pristine and functionalized MXenes. DFT calculations were performed using the Vienna *ab-initio* simulation package (VASP)[44, 45] based on the PAW method. The wave-function was converged to a threshold of 10^{-5} eV with a plane-wave energy cut-off set to 500 eV and a k-point mesh of $15 \times 15 \times 1$ following the Monkhorst Pack method for 2D structures. The geometry of all structures were optimized to converge the interatomic forces below a threshold of 0.01 eV/Å using the generalized gradient approximation (GGA) PBE[46] exchange-correlation functional; the dispersion forces have been described using the DFT-D3 method[47]. The MXenes unit cell was obtained

from the corresponding MAX phase bulk structure, by cutting the M_2C slab perpendicular to the $\langle 001 \rangle$ direction and adding a vacuum region of 15 Å. To improve the generally underestimated band gaps by GGA methods[18], the band structure and projected density of states (PDOS) were obtained with the hybrid HSE06[48] functional. The work function (WF) was derived from the energy difference between the Fermi level and the vacuum level[34].

Most MXenes have the high-symmetry $P\bar{3}1m$ space group[14, 31, 49]. In our case, the symmetry of bimetallic and vacancy-ordered MXenes is lower than that of the V_2C MXene due to the presence of Zr atoms (or vacancy). To accurately assess the band structure and phonon dispersion of MXenes, we expanded the definition of symmetry points of the hexagonal Brillouin zone (see Figure S1), thus breaking the degeneracy of M and K points and naming the now inequivalent points as M1, K1, M2, K2, M3, K3, as previously reported for $(Mo_{2/3}□_{1/3})_2CX_2$ [43]. The energy difference at symmetry points is significant and therefore cannot be disregarded. All band structures are in the electronic supplementary information.

The vibrational properties within the harmonic approximation are entirely defined within the dynamical matrix (Hessian matrix) calculated at the density functional perturbation theory (DFPT)[50] level as implemented in VASP. The post-processing and analysis has thus been performed using the software PhonoPy[51]. The convergence standards have been increased to 10^{-7} eV and to 10^{-6} eV/Å for the wave-function and interatomic forces, respectively. The other parameters have been kept consistent with the geometry optimization.

To evaluate the stability of functionalized $(V_{2/3}Zr_{1/3})_2CX_2$ MXenes, the formation energy (E_{form}) of the unit cell is calculated as:

$$E_{form} = \frac{(E[(V_{2/3}Zr_{1/3})_2CX_2] - E[(V_{2/3}Zr_{1/3})_2C]) - E[X_g]}{3} \quad (1)$$

where $E[(V_{2/3}Zr_{1/3})_2C]$ and $E[(V_{2/3}Zr_{1/3})_2CX_2]$ stand for the total energies of pristine $(V_{2/3}Zr_{1/3})_2C$ and functionalized $(V_{2/3}Zr_{1/3})_2CX_2$, respectively. $E[X_g]$ is the energy of O_2 , F_2 and H_2O molecules in the gas phase and $E[OH] = E[H_2O] - \frac{1}{2}E[H_2]$.

For a quick assessment of structural stability, we considered a set of *ab-initio* molecular dynamics (AIMD), as implemented in VASP. These simulations have been completed using the Nosé algorithm[52] in the NVT ensemble at room temperature (300 K) for 9 ps.

We used a scalar, collinear magnetic model, and we considered the ferromagnetic (FM) configuration and the three possible antiferromagnetic (AFM) states to calculate the preferred magnetic ground state structures of $(V_{2/3}Zr_{1/3})_2CX_2$ system (Figure S2). To comprehensively assess the magnetic behavior of these MXenes, we have constructed an Ising model (see Figure S3) using exchange coupling parameters derived from DFT simulations. This allowed us to calculate the Curie temperature by Monte Carlo simulations (see Section 3.2.3) performed with the open-source software ALPS[53].

3 Result and discussion

3.1 Structural analysis

MXene structures derive from corresponding bulk MAX phases, as shown in Figure 1. The pristine $(V_{2/3}Zr_{1/3})_2C$ MXene slab is formed (upon removal of the Al layer) by three hexagonal layers stacked on top of each other, and the layer of C atoms is sandwiched between layers composed of V and Zr atoms (Figure 1b). The Zr atoms are all aligned along the short diagonal of the *ab*-plane. Functionalized MXenes are obtained by surface termination (F, OH, or O termination), while vacancy-ordered MXenes are obtained by removing Zr atoms. The structural details (e.g., lattice constant, bond lengths, etc.) are outlined in Table S1.

Our calculations suggest that the bimetallic $(V_{2/3}Zr_{1/3})_2C$ MXene can be obtained from a parent $(V_{2/3}Zr_{1/3})_2AlC$ MAX phase. First, the calculated exfoliation energy of $(V_{2/3}Zr_{1/3})_2CAI$ is very similar to that of V_2AlC [54] (2.59 J/m² versus 2.53 J/m², respectively, as shown in Figure S4). Second, the absence of soft modes at the Γ -point, as shown by the dispersion of the vibrational modes, ensures the dynamical stability of the structure, which is further supported by AIMD calculations performed at 300 K for $(V_{2/3}Zr_{1/3})_2C$ (Figure S5). All these results indicate that bimetallic MXene is kinetically stable and can be obtained experimentally, similarly to V_2C [55].

The stability and other properties of MXenes depend on surface functionalization, which in turn depends on the exfoliation process. Experimental investigation of related V_2C MXenes[56] has shown that different conditions (i.e. solvent, O_2 partial pressure, etc) during the exfoliation process, lead to different surface decorations[7, 27, 57]. In analogy to the study by Harris *et al.*, we selected the following surface functional groups: O, F and OH. The functional groups are positioned above the *hollow* site formed by three neighbouring C mirroring the positions of the metals on the

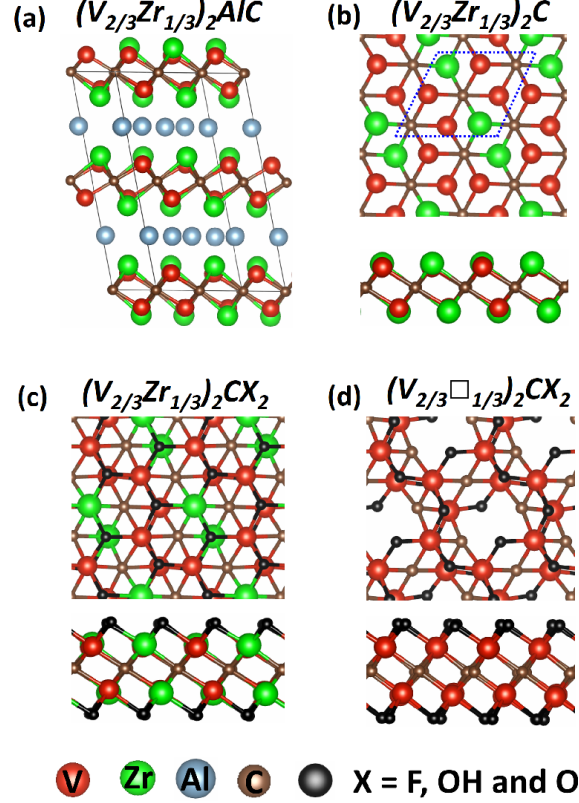


Figure 1: Structures of parent MAX phase $(V_{2/3}Zr_{1/3})_2AlC$ (a), pristine bimetallic MXene $(V_{2/3}Zr_{1/3})_2C$ (b), functionalized bimetallic MXene $(V_{2/3}Zr_{1/3})_2CX_2$ (c) and vacancy-ordered $(V_{2/3}\square_{1/3})_2CX_2$ ($X = F, OH$ and O) MXene (d). The unit cell of MXenes is marked by a blue dotted line.

opposite layer. Such structures are systematically more stable than structures with functional groups sitting on top of the C atoms (Figure S6).

The formation energies of $(V_{2/3}Zr_{1/3})_2CX_2$ -functionalized MXenes calculated from Equation 1 are large, -5.21 , -7.55 and -4.48 eV for $X = F, OH$ and O , respectively, thus highlighting the formation of strong chemical bonds on MXene surfaces (V or Zr atoms). This is also supported by AIMD simulation at 300K (Figure S7). However, when removing Zr, the $(V_{2/3}\square_{1/3})_2C$ and $(V_{2/3}\square_{1/3})_2CO_2$ structures are subjected to large interatomic forces and heavily distorted during just a short AIMD simulation. We also found that only $(V_{2/3}\square_{1/3})_2CF_2$ and $(V_{2/3}\square_{1/3})_2C(OH)_2$ are kinetically stable, based on both AIMD and phonon spectra calculations (Figure S8). Thus, the interaction between metals and surface functional groups is weaker in vacancy-ordered MXenes than in bimetallic MXenes.

3.2 Magnetic and electronic properties

3.2.1 Bimetallic MXenes

Due to the super-exchange mechanism[58], $(V_{2/3}Zr_{1/3})_2C$ exhibits an antiferromagnetic behaviour. This can be seen in the spin-polarized charge densities and in electron localization functions (ELF) plotted in (Figure 2a).

Electronic Local Function (ELF) maps show that $(V_{2/3}Zr_{1/3})_2C$ has distinct characteristics of electrons localized on V atoms, which leads to the super-exchange mechanism. The band structure of $(V_{2/3}Zr_{1/3})_2C$ shows a semiconducting character with a band gap of 0.78 eV (Figure S8), and PDOS shown in Figure 2c are in line with ELF. The states near CBM and VBM have main contributions from the V $3d$ orbitals, while the contributions from Zr $3d$ orbitals and C $2p$ orbitals are insignificant.

The magnetic properties of $(V_{2/3}Zr_{1/3})_2CO_2$ are qualitatively different. The presence of surface oxygens changes the magnetic ordering, resulting in FM ground state with $\Delta E = E_{AFM} - E_{FM}$ of 33.59 meV/unit cell with respect to

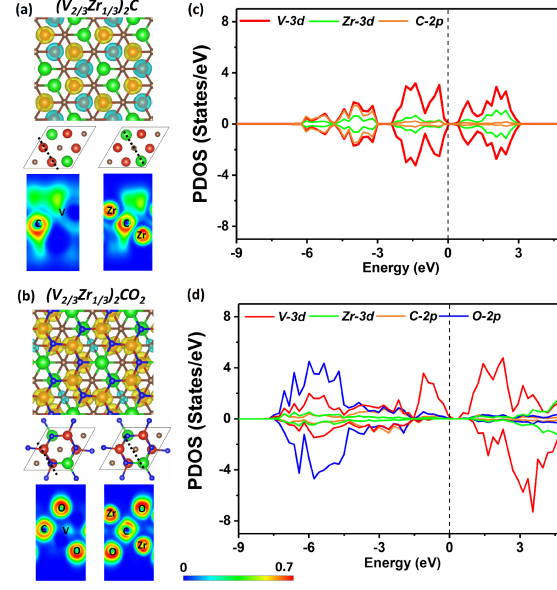


Figure 2: Spin polarized charge densities and electron localization function (ELF) maps (perpendicular to (001) direction) are shown for $(V_{2/3}Zr_{1/3})_2C$ (a) and $(V_{2/3}Zr_{1/3})_2CO_2$ (b), where spin up and spin down densities are shown in yellow and light blue, respectively. The units of color scale is "probability". Project density of states (PDOS) of $(V_{2/3}Zr_{1/3})_2C$ (c) and $(V_{2/3}Zr_{1/3})_2CO_2$ (d). Fermi level (black dotted line) is set to zero.

the most stable AFM state. The total magnetic moment of $(V_{2/3}Zr_{1/3})_2CO_2$ is $4 \mu_B$ per unit cell. d -electrons of V atoms can induce the spin-polarization of the neighbouring C atoms via double-exchange mechanism [59](Figure 2b). The presence of oxygens on the MXene surface also leads to charge transfer towards the surface (as shown by Bader charge analysis[60], Table S1), and this affects the position of the V $3d$ in the spin-down channel (see PDOS, Figure 2d), which is shifted down in energy and no longer participates in VBM. However, surface oxygens have no effect on the spin-up channel. This is reflected on the band structure, which exhibits distinct half-semiconductor features. The two half-semiconducting gaps are 0.53 and 1.85 eV for spin-up and spin-down channels (Figure S8), respectively. The difference of the band edge energy between the two spin channels ($\Delta E_{CBM} = E_{CBM(down)} - E_{CBM(up)}$) and $\Delta E_{VBM} = E_{VBM(down)} - E_{VBM(up)}$) shows the typical half-semiconducting character (See Table S2 for complete set of characteristics).

Both $(V_{2/3}Zr_{1/3})_2CF_2$ and $(V_{2/3}Zr_{1/3})_2C(OH)_2$ MXenes exhibits similar magnetic properties, and only the results regarding the former are discussed here (see Figure S9 for further details on the latter). The $(V_{2/3}Zr_{1/3})_2CF_2$ MXene exhibits an AFM magnetic character, similarly to pristine $(V_{2/3}Zr_{1/3})_2C$. The AFM magnetic configuration is remarkably stable, showing $\Delta E = -841.08$ meV. Such analogous value has already been reported for V_2CF_2 [61]. The analysis of spin-polarized densities and ELF suggests that $(V_{2/3}Zr_{1/3})_2C(OH)_2$ MXene shows an analogous behaviour to the pristine MXene, i.e., super-exchange mechanism. The presence of F surface atoms widens the band gap due to electron density localization around the halide centre, in analogy to the O-terminated surface. However, the FM state is not stabilized in $(V_{2/3}Zr_{1/3})_2CF_2$ since both V $3d$ spin channels are equally shifted (Figure 3a and c).

3.2.2 Vacancy-ordered MXene

The pristine $(V_{2/3}\square_{1/3})_2C$ MXene is unstable and therefore cannot be directly compared to the pristine bimetallic MXene. Only the F-functionalized MXene can be directly compared to the pristine $(V_{2/3}\square_{1/3})_2C$ MXene. In contrast to $(V_{2/3}Zr_{1/3})_2CF_2$, the FM phase of $(V_{2/3}\square_{1/3})_2CF_2$ is the most stable, with a ΔE of 22.93 meV. The reduced presence of metals induces an overall magnetic moment of $2 \mu_B$, with the unpaired spins localized on V atoms (Figure 3b).

The FM ordering results from the effect of V d -electrons, which induce spin-polarization of neighbouring C atoms via a double-exchange mechanism, as shown by the ELF map in Figure 3b. The band structure shows a half-semiconducting behaviour (Figure S8), which originates from the spin-polarization of CBM observed in $(V_{2/3}\square_{1/3})_2CF_2$. We can also observe a smaller polarization on VBM, due to the slight shift in the PDOS of the V $3d$ orbitals in the spin-down channel. The full set of electronic properties are outlined in Table S2. The polarization of the band edges can be explained by PDOS, wherein, in addition to the V $3d$ orbital, C and F orbitals also significantly contribute to the VBM

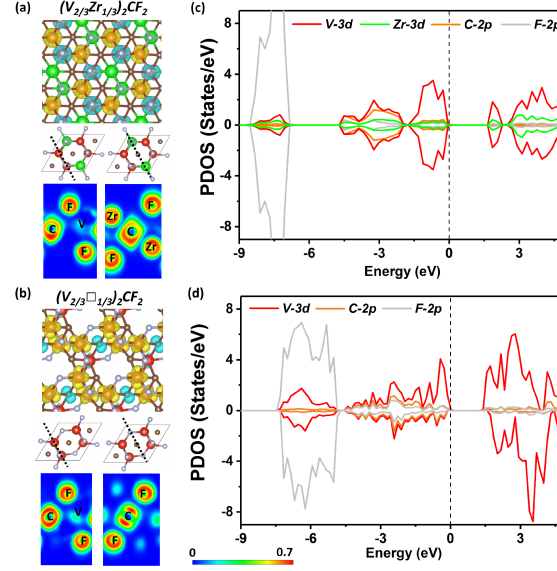


Figure 3: (a) and (b) The inserted background figure shows spin-polarized charge densities on $(V_{2/3}Zr_{1/3})_2CF_2$ and $(V_{2/3}\square_{1/3})_2CF_2$, where spin up and spin down densities are shown in yellow and light blue, respectively. The sections (dot lines) of electron localization function (ELF) maps are perpendicular to (001) direction. The units of color scale is "probability". (e) and (f) The project density of states (PDOS) of $(V_{2/3}Zr_{1/3})_2CF_2$ and $(V_{2/3}\square_{1/3})_2CF_2$. Fermi level is set up to zero with the black dotted line.

(3d). We also considered the $(V_{2/3}\square_{1/3})_2C(OH)_2$, which behaves similarly to $(V_{2/3}\square_{1/3})_2CF_2$; however, due to the lower electronegativity of OH, the effect of spin polarization is weaker and hence ΔE is smaller.

3.2.3 Curie temperatures

Curie temperatures were calculated for MXene with FM ground state - $(V_{2/3}Zr_{1/3})_2CO_2$, $(V_{2/3}\square_{1/3})_2CF_2$ and $(V_{2/3}\square_{1/3})_2C(OH)_2$ - using the Monte Carlo simulations. The temperature evolution of magnetic momentum per unit cell is shown in Figure 4. The phase transition between the FM and paramagnetic states for $(V_{2/3}Zr_{1/3})_2CO_2$ occurs around room temperature with an estimated T_C of 270 K. This is significantly different from $(V_{2/3}\square_{1/3})_2CF_2$ and $(V_{2/3}\square_{1/3})_2C(OH)_2$ MXenes where the transitions occur around 26 and 10 K, respectively. This is due to a weaker magnetic interaction upon the Zr atom removal.

3.2.4 Work function

The WF of MXenes strongly depends on stoichiometry and surface functionalization (see Figure 5), which makes it possible to obtain materials which can be used as either electron emitters with low WF or contacts without Schottky barrier and high work-function[33, 34]. The presence of electron-rich Zr in $(V_{2/3}Zr_{1/3})_2C$ MXene shifts the Fermi level and lower the WF from 4.30 eV with respect to V_2C to 3.90 eV. Surface functionalization affects the electrostatic potential charge near the surfaces[34, 35], thereby increasing the WF of $(V_{2/3}Zr_{1/3})_2C$ MXene to 5.83 and 5.32 eV when the surface is terminated with O or F, respectively. A different effect is observed in the OH surface termination, where the WF is decreased to 1.37 eV due to the intrinsic dipole of the OH group. This value is lower than that previously reported for $Sc_2C(OH)_2$ MXene (1.60 eV)[34]. Therefore, $(V_{2/3}Zr_{1/3})_2C(OH)_2$ MXene is a candidate for low-WF emitting cathodes. Removing the Zr atoms increases the WF to 7.47 and 4.16 eV for $(V_{2/3}\square_{1/3})_2CF_2$ and $(V_{2/3}\square_{1/3})_2C(OH)_2$ MXenes, respectively. Our analysis clearly shows that the WF of various $(V_{2/3}Zr_{1/3})_2C$ MXenes investigated herein can be tuned within a broad range of values; the $(V_{2/3}Zr_{1/3})_2C(OH)_2$ MXene could be used as an ultra-low work function electron emitter. It's interesting to note that the $(V_{2/3}\square_{1/3})_2CF_2$ MXene has a higher WF than the Pt metal (which has the highest WF among the elemental metals[33]), it could be used for hole injection in Schottky-barrier-free contact applications.

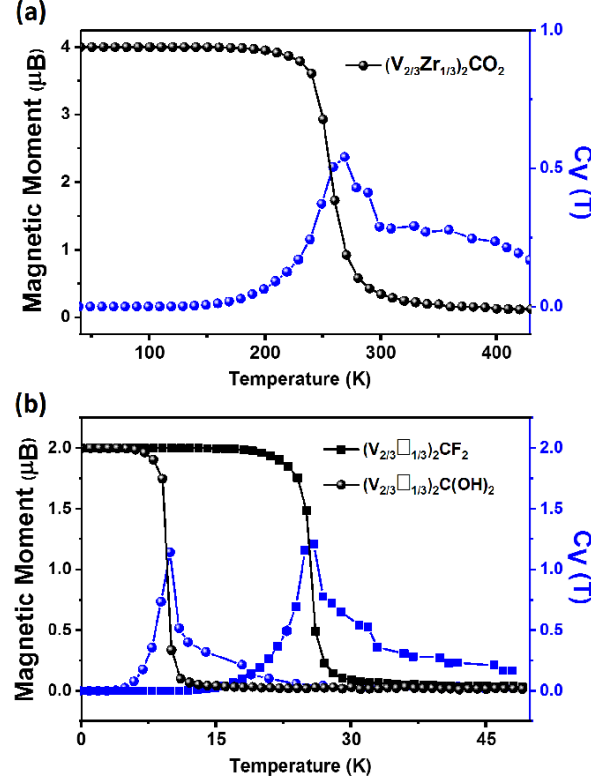


Figure 4: Variation of the total magnetic momentum (per unit cell) of (a) $(V_{2/3}Zr_{1/3})_2CO_2$ (b) $(V_{2/3}\square_{1/3})_2CF_2$ and $(V_{2/3}\square_{1/3})_2C(OH)_2$ with respect to the temperature. Corresponding specific heats C_V are shown in blue.

4 Conclusions

Our results show that modifying the stoichiometry and/or surface functionalization of MXenes changes their properties qualitatively. Therefore they are excellent candidates for applications in spintronics because their electric and magnetic properties can be tuned for specific purposes. In this study, we identified $(V_{2/3}Zr_{1/3})_2CX_2$, $(V_{2/3}\square_{1/3})_2CF_2$ and $(V_{2/3}\square_{1/3})_2C(OH)_2$ as stable candidates. Among them, the $(V_{2/3}Zr_{1/3})_2CO_2$ and $(V_{2/3}\square_{1/3})_2CF_2$ and $(V_{2/3}\square_{1/3})_2C(OH)_2$ are half-semiconductor materials. The predicted Curie temperature for $(V_{2/3}Zr_{1/3})_2CO_2$ (270 K) is higher than that of the experimentally reported 2D CrI_3 crystals (45 K).[16] Hence, of the MXenes tested in this study, $(V_{2/3}Zr_{1/3})_2CO_2$ is the best candidate for spintronic applications.

The functional groups of MXenes can radically change the composition of their frontier orbitals, thereby affecting their work function. In particular, we found that $(V_{2/3}Zr_{1/3})_2C(OH)_2$ MXene can be used as an ultra-low work function electron emitter and its work function (1.37 eV) is lower than that of $Sc_2C(OH)_2$ MXene (1.6 eV), as reported by Khazaei *et al.*. Conversely, the $(V_{2/3}\square_{1/3})_2CF_2$ MXene has a rather high WF of 7.47 eV, which is thus higher than that of the Pt metal[33]. Thanks to these properties, $(V_{2/3}\square_{1/3})_2CF_2$ MXenes can be used for holes injection in applications requiring Schottky-barrier-free contacts. Therefore, $(V_{2/3}Zr_{1/3})_2C(OH)_2$ and vacancy-ordered $(V_{2/3}\square_{1/3})_2CF_2$ MXenes are also promising candidates for electronic devices.

Overall, the results presented in this study establish a new family of MXenes with intrinsic magnetism, which makes them ideal candidates for both spintronic and electronic applications in the near future.

5 Acknowledgements

A support from OP VVV "Excellent Research Teams", project CUCAM, is also acknowledged. J. H. acknowledges the financial support provided by the National Natural Science Foundation of China (Grant No. 11804041). S. L. acknowledges the support from GAUK project (Grant No. 792218). Thanks Carlos V. Melo for his precious contribution of writing guidance.

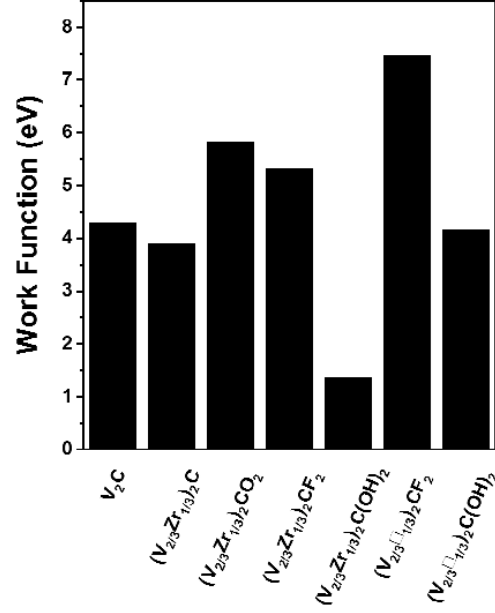


Figure 5: Work functions of V_2C , pristine $(V_{2/3}Zr_{1/3})_2C$, bimetallic $(V_{2/3}Zr_{1/3})_2CX_2$ and vacancy-ordered $(V_{2/3}\square_{1/3})_2CX_2$ MXenes

References

- [1] Kostya S Novoselov, Andre K Geim, Sergei V Morozov, D Jiang, Y_ Zhang, Sergey V Dubonos, Irina V Grigorieva, and Alexandr A Firsov. Electric field effect in atomically thin carbon films. *Science*, 306(5696):666–669, 2004.
- [2] Yi Lin, Tiffany V Williams, and John W Connell. Soluble, exfoliated hexagonal boron nitride nanosheets. *The Journal of Physical Chemistry Letters*, 1(1):277–283, 2009.
- [3] Boubekour Lalmi, Hamid Oughaddou, Hanna Enriquez, Abdelkader Kara, Sébastien Vizzini, Bénédicte Ealet, and Bernard Aufray. Epitaxial growth of a silicene sheet. *Applied Physics Letters*, 97(22):223109, 2010.
- [4] Manish Chhowalla, Hyeon Suk Shin, Goki Eda, Lain-Jong Li, Kian Ping Loh, and Hua Zhang. The chemistry of two-dimensional layered transition metal dichalcogenide nanosheets. *Nature Chemistry*, 5(4):263, 2013.
- [5] Manish Chhowalla, Zhongfan Liu, and Hua Zhang. Two-dimensional transition metal dichalcogenide (tmd) nanosheets. *Chemical Society Reviews*, 44(9):2584–2586, 2015.
- [6] Han Liu, Yuchen Du, Yexin Deng, and D Ye Peide. Semiconducting black phosphorus: synthesis, transport properties and electronic applications. *Chemical Society Reviews*, 44(9):2732–2743, 2015.
- [7] Michael Naguib, Vadym N Mochalin, Michel W Barsoum, and Yury Gogotsi. 25th anniversary article: Mxenes: a new family of two-dimensional materials. *Advanced Materials*, 26(7):992–1005, 2014.
- [8] Hua Zhang. Ultrathin two-dimensional nanomaterials. *ACS Nano*, 9(10):9451–9469, 2015.
- [9] Igor Žutić, Jaroslav Fabian, and S Das Sarma. Spintronics: Fundamentals and applications. *Reviews of Modern Physics*, 76(2):323, 2004.
- [10] Albert Fert, Nicolas Reyren, and Vincent Cros. Magnetic skyrmions: advances in physics and potential applications. *Nature Reviews Materials*, 2(7):17031, 2017.
- [11] AH Castro Neto, Francisco Guinea, Nuno MR Peres, Kostya S Novoselov, and Andre K Geim. The electronic properties of graphene. *Reviews of Modern Physics*, 81(1):109, 2009.
- [12] Zhong Lin, Amber McCreary, Natalie Briggs, Shruti Subramanian, Kehao Zhang, Yifan Sun, Xufan Li, Nicholas J Borys, Hongtao Yuan, Susan K Fullerton-Shirey, et al. 2d materials advances: from large scale synthesis and controlled heterostructures to improved characterization techniques, defects and applications. *2D Materials*, 3(4):042001, 2016.
- [13] Engin Torun, H Sahin, SK Singh, and FM Peeters. Stable half-metallic monolayers of fecl2. *Applied Physics Letters*, 106(19):192404, 2015.

- [14] Chen Si, Jian Zhou, and Zhimei Sun. Half-metallic ferromagnetism and surface functionalization-induced metal–insulator transition in graphene-like two-dimensional cr₂c crystals. *ACS Applied Materials & Interfaces*, 7(31):17510–17515, 2015.
- [15] Cheng Gong, Lin Li, Zhenglu Li, Huiwen Ji, Alex Stern, Yang Xia, Ting Cao, Wei Bao, Chenzhe Wang, Yuan Wang, et al. Discovery of intrinsic ferromagnetism in two-dimensional van der waals crystals. *Nature*, 546(7657):265, 2017.
- [16] Bevin Huang, Genevieve Clark, Efrén Navarro-Moratalla, Dahlia R Klein, Ran Cheng, Kyle L Seyler, Ding Zhong, Emma Schmidgall, Michael A McGuire, David H Cobden, et al. Layer-dependent ferromagnetism in a van der waals crystal down to the monolayer limit. *Nature*, 546(7657):270, 2017.
- [17] Guoying Gao, Guangqian Ding, Jie Li, Kailun Yao, Menghao Wu, and Meichun Qian. Monolayer mxenes: promising half-metals and spin gapless semiconductors. *Nanoscale*, 8(16):8986–8994, 2016.
- [18] Junjie He, Pengbo Lyu, and Petr Nachtigall. New two-dimensional mn-based mxenes with room-temperature ferromagnetism and half-metallicity. *Journal of Materials Chemistry C*, 4(47):11143–11149, 2016.
- [19] Siham Ouardi, Gerhard H Fecher, Claudia Felser, and Jürgen Kübler. Realization of spin gapless semiconductors: The heusler compound mn₂ coal. *Physical Review Letters*, 110(10):100401, 2013.
- [20] XL Wang. Proposal for a new class of materials: spin gapless semiconductors. *Physical Review Letters*, 100(15):156404, 2008.
- [21] Xingxing Li, Xiaojun Wu, Zhenyu Li, Jinlong Yang, and JG Hou. Bipolar magnetic semiconductors: a new class of spintronics materials. *Nanoscale*, 4(18):5680–5685, 2012.
- [22] Wei-Bing Zhang, Qian Qu, Peng Zhu, and Chi-Hang Lam. Robust intrinsic ferromagnetism and half semi-conductivity in stable two-dimensional single-layer chromium trihalides. *Journal of Materials Chemistry C*, 3(48):12457–12468, 2015.
- [23] Junyi Liu, Qiang Sun, Yoshiyuki Kawazoe, and Puru Jena. Exfoliating biocompatible ferromagnetic cr-trihalide monolayers. *Physical Chemistry Chemical Physics*, 18(13):8777–8784, 2016.
- [24] Min Kan, Subash Adhikari, and Qiang Sun. Ferromagnetism in mn_x 2 (x= s, se) monolayers. *Physical Chemistry Chemical Physics*, 16(10):4990–4994, 2014.
- [25] Xingxing Li and Jinlong Yang. First-principles design of spintronics materials. *National Science Review*, 3(3):365–381, 2016.
- [26] D Zhong. D. zhong, kl seyler, x. linpeng, r. cheng, n. sivadas, b. huang, e. schmidgall, t. taniguchi, k. watanabe, ma mcguire, w. yao, d. xiao, k.-mc fu, and x. xu, sci. adv. 3, e1603113 (2017). *Science Advances*, 3:e1603113, 2017.
- [27] Michael Naguib, Murat Kurtoglu, Volker Presser, Jun Lu, Junjie Niu, Min Heon, Lars Hultman, Yury Gogotsi, and Michel W Barsoum. Two-dimensional nanocrystals produced by exfoliation of ti₃alc₂. *Advanced Materials*, 23(37):4248–4253, 2011.
- [28] Michael Naguib, Olha Mashtalir, Joshua Carle, Volker Presser, Jun Lu, Lars Hultman, Yury Gogotsi, and Michel W Barsoum. Two-dimensional transition metal carbides. *ACS Nano*, 6(2):1322–1331, 2012.
- [29] Vincent Ming Hong Ng, Hui Huang, Kun Zhou, Pooi See Lee, Wenxiu Que, Jason Zhichuan Xu, and Ling Bing Kong. Recent progress in layered transition metal carbides and/or nitrides (mxenes) and their composites: synthesis and applications. *Journal of Materials Chemistry A*, 5(7):3039–3068, 2017.
- [30] Jin-Cheng Lei, Xu Zhang, and Zhen Zhou. Recent advances in mxene: Preparation, properties, and applications. *Frontiers of Physics*, 10(3):276–286, 2015.
- [31] Junjie He, Guangqian Ding, Chengyong Zhong, Shuo Li, Dengfeng Li, and Gang Zhang. Cr₂ tic₂-based double mxenes: novel 2d bipolar antiferromagnetic semiconductor with gate-controllable spin orientation toward antiferromagnetic spintronics. *Nanoscale*, 11(1):356–364, 2019.
- [32] Arni Sigurdur Ingason, Martin Dahlqvist, and Johanna Rosén. Magnetic max phases from theory and experiments; a review. *Journal of Physics: Condensed Matter*, 28(43):433003, 2016.
- [33] Yuanyue Liu, Hai Xiao, and William A Goddard III. Schottky-barrier-free contacts with two-dimensional semiconductors by surface-engineered mxenes. *Journal of the American Chemical Society*, 138(49):15853–15856, 2016.
- [34] Mohammad Khazaei, Masao Arai, Taizo Sasaki, Ahmad Ranjbar, Yunye Liang, and Seiji Yunoki. Oh-terminated two-dimensional transition metal carbides and nitrides as ultralow work function materials. *Physical Review B*, 92(7):075411, 2015.

- [35] Mohammad Khazaei, Ahmad Ranjbar, Mahdi Ghorbani-Asl, Masao Arai, Taizo Sasaki, Yunye Liang, and Seiji Yunoki. Nearly free electron states in mxenes. *Physical Review B*, 93(20):205125, 2016.
- [36] Byoung-Chul Min, Kazunari Motohashi, Cock Lodder, and Ron Jansen. Tunable spin-tunnel contacts to silicon using low-work-function ferromagnets. *Nature Materials*, 5(10):817, 2006.
- [37] Yasunobu Ando, Yoshihiro Gohda, and Shinji Tsuneyuki. Dependence of the schottky barrier on the work function at metal/silicon(0001) interfaces identified by first-principles calculations. *Surface Science*, 606(19-20):1501–1506, 2012.
- [38] JL Freeouf and JM Woodall. Schottky barriers: An effective work function model. *Applied Physics Letters*, 39(9):727–729, 1981.
- [39] Quanzheng Tao, Martin Dahlqvist, Jun Lu, Sankalp Kota, Rahele Meshkian, Joseph Halim, Justinas Palisaitis, Lars Hultman, Michel W Barsoum, Per OÅ Persson, et al. Two-dimensional mo_{1.33}c mxene with divacancy ordering prepared from parent 3d laminate with in-plane chemical ordering. *Nature Communications*, 8:14949, 2017.
- [40] Andreas Thore and Johanna Rosén. An investigation of the in-plane chemically ordered atomic laminates (mo_{2/3}sc_{1/3})₂alc and (mo_{2/3}y_{1/3})₂alc from first principles. *Physical Chemistry Chemical Physics*, 19(32):21595–21603, 2017.
- [41] Mohammad Khazaei, Vei Wang, Cem Sevik, Ahmad Ranjbar, Masao Arai, and Seiji Yunoki. Electronic structures of imax phases and their two-dimensional derivatives: A family of piezoelectric materials. *Physical Review Materials*, 2(7):074002, 2018.
- [42] Martin Dahlqvist, Jun Lu, Rahele Meshkian, Quanzheng Tao, Lars Hultman, and Johanna Rosen. Prediction and synthesis of a family of atomic laminate phases with kagomé-like and in-plane chemical ordering. *Science Advances*, 3(7):e1700642, 2017.
- [43] Hans Lind, Joseph Halim, SI Simak, and Johanna Rosén. Investigation of vacancy-ordered mo_{1.33}c mxene from first principles and x-ray photoelectron spectroscopy. *Physical Review Materials*, 1(4):044002, 2017.
- [44] G Kresse. G. kresse and j. hafner, phys. rev. b 47, 558 (1993). *Physical Review B*, 47:558, 1993.
- [45] G Kresse. G. kresse and d. joubert, phys. rev. b 59, 1758 (1999). *Physical Review B*, 59:1758, 1999.
- [46] John P Perdew, Kieron Burke, and Matthias Ernzerhof. Generalized gradient approximation made simple. *Physical Review Letters*, 77(18):3865, 1996.
- [47] Stefan Grimme, Jens Antony, Stephan Ehrlich, and Helge Krieg. A consistent and accurate ab initio parametrization of density functional dispersion correction (dft-d) for the 94 elements h-pu. *The Journal of Chemical Physics*, 132(15):154104, 2010.
- [48] Jochen Heyd, Gustavo E Scuseria, and Matthias Ernzerhof. Hybrid functionals based on a screened coulomb potential. *The Journal of Chemical Physics*, 118(18):8207–8215, 2003.
- [49] Nathan C Frey, Arkamita Bandyopadhyay, Hemant Kumar, Babak Anasori, Yury Gogotsi, and Vivek B Shenoy. Surface engineered mxenes: Electric field control of magnetism and enhanced magnetic anisotropy. *ACS Nano*, 2019.
- [50] Stefano Baroni, Stefano De Gironcoli, Andrea Dal Corso, and Paolo Giannozzi. Phonons and related crystal properties from density-functional perturbation theory. *Reviews of Modern Physics*, 73(2):515, 2001.
- [51] Atsushi Togo and Isao Tanaka. First principles phonon calculations in materials science. *Scripta Materialia*, 108:1–5, 2015.
- [52] Shuichi Nosé. A unified formulation of the constant temperature molecular dynamics methods. *The Journal of Chemical Physics*, 81(1):511–519, 1984.
- [53] A Fabricio Albuquerque, Fabien Alet, Philippe Corboz, Prakash Dayal, Adrian Feiguin, S Fuchs, L Gamper, E Gull, S Gürtler, Andreas Honecker, et al. The alps project release 1.3: Open-source software for strongly correlated systems. *Journal of Magnetism and Magnetic Materials*, 310(2):1187–1193, 2007.
- [54] Zhonglu Guo, Jian Zhou, and Zhimei Sun. New two-dimensional transition metal borides for li ion batteries and electrocatalysis. *Journal of Materials Chemistry A*, 5(45):23530–23535, 2017.
- [55] Fanfan Liu, Jie Zhou, Shuwei Wang, Bingxin Wang, Cai Shen, Libo Wang, Qianku Hu, Qing Huang, and Aiguo Zhou. Preparation of high-purity v₂c mxene and electrochemical properties as li-ion batteries. *Journal of The Electrochemical Society*, 164(4):A709–A713, 2017.

- [56] Kristopher J Harris, Matthieu Bugnet, Michael Naguib, Michel W Barsoum, and Gillian R Goward. Direct measurement of surface termination groups and their connectivity in the 2d mxene v2ct x using nmr spectroscopy. *The Journal of Physical Chemistry C*, 119(24):13713–13720, 2015.
- [57] Mohammad Khazaei, Masao Arai, Taizo Sasaki, Chan-Yeup Chung, Natarajan S Venkataramanan, Mehdi Estili, Yoshio Sakka, and Yoshiyuki Kawazoe. Novel electronic and magnetic properties of two-dimensional transition metal carbides and nitrides. *Advanced Functional Materials*, 23(17):2185–2192, 2013.
- [58] Junjiro Kanamori. Superexchange interaction and symmetry properties of electron orbitals. *Journal of Physics and Chemistry of Solids*, 10(2-3):87–98, 1959.
- [59] P-G De Gennes. Effects of double exchange in magnetic crystals. *Physical Review*, 118(1):141, 1960.
- [60] Graeme Henkelman, Andri Arnaldsson, and Hannes Jónsson. A fast and robust algorithm for bader decomposition of charge density. *Computational Materials Science*, 36(3):354–360, 2006.
- [61] Junping Hu, Bo Xu, Chuying Ouyang, Shengyuan A Yang, and Yugui Yao. Investigations on v2c and v2cx2 (x= f, oh) monolayer as a promising anode material for li ion batteries from first-principles calculations. *The Journal of Physical Chemistry C*, 118(42):24274–24281, 2014.

Control of spintronic and electronic properties of bimetallic and vacancy-ordered vanadium carbide MXenes via surface functionalization

Shuo Li,^a Junjie He,^b Petr Nachtigall,^a Lukáš Grajciar,^a Federico Brivio ^{*a}

September 7, 2021

1 Ising model

DFT results do not take into account magnetic properties with respect to temperature and scale-effect. To take in account for these effects we used a simple Ising model. We considered a scalar, collinear magnetic model. We considered the ferromagnetic (FM) configuration and the three possible antiferromagnetic (AFM) states to calculate the preferred magnetic ground state structures of $(V_{2/3}Zr_{1/3})_2CX_2$ system.

In order to obtain the full magnetic behavior it is necessary to use larger simulation as the Ising model. it is necessary to map the the energy landscape to an effective classical spin Hamiltonian on a honeycomb lattice accordingly to

$$H_{spin} = \frac{1}{2} \sum_{i \neq j} J_{ij} S_i \cdot S_j \quad (1)$$

where S_i is the total spin magnetic moment of the atomic site i , J_{ij} are the exchange coupling parameters between two local spins, and the prefactor $1/2$ accounts for the double counting of spin. We can extract the nearest-neighbor (J_1), second-nearest-neighbor (J_2), and third-nearest-neighbor (J_3) coupling constants from DFT simulations (see Figure S3).

$$E_{FM} - E_{AFM1} = (J_2 + J_3)S^2 \quad (2)$$

$$E_{AFM1} - E_{AFM2} = (J_1 - J_3)S^2 \quad (3)$$

$$E_{FM} + E_{AFM1} - E_{AFM2} - E_{AFM3} = 2J_1S^2 \quad (4)$$

where $S = 1$ corresponds to the V^{2+} configuration.

^aDepartment of Physical and Macromolecular Chemistry, Faculty of Science, Charles University in Prague, 128 43 Prague 2, Czech Republic; E-mail: briviof@natur.cuni.cz

^bBremen Center for Computational Materials Science, University of Bremen, Am Fallturm 1, 28359 Bremen, Germany

2 Figures

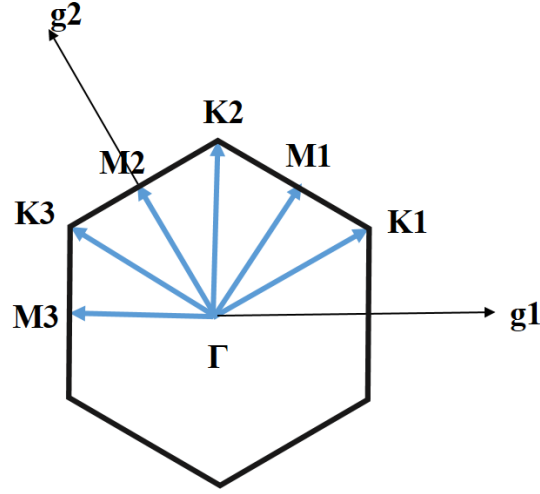


Figure S1: A schematic representation of the Brillouin zone of a 2D hexagonal lattice, along with an expansion of symmetry points for the reduced symmetry of $(V_{2/3}Zr_{1/3})_2CX_2$ and $(V_{2/3}\square_{1/3})_2CX_2$. The black line demonstrates the path used in the band structure diagrams going in order of Γ -M1-K1- Γ -M2-K2- Γ -M3-K3- Γ . g_1 and g_2 are the basis vectors.

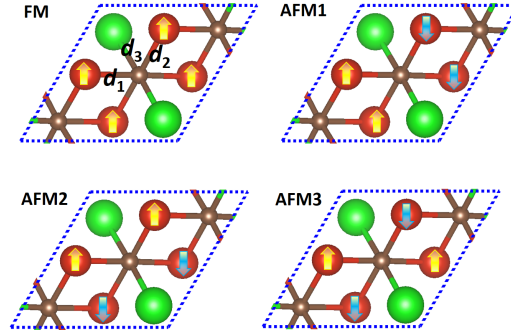


Figure S2: FM and different AFM states are presented. d_1 , d_2 and d_3 are bond length of C-V and C-Zr.

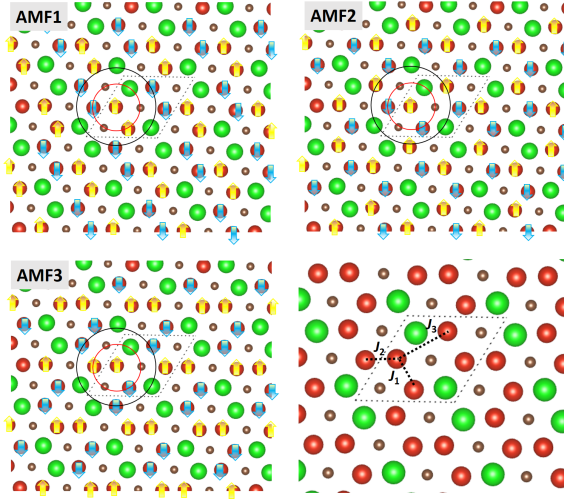


Figure S3: To define the nearest-neighbor (J_1), second-nearest-neighbor (J_2), and third-nearest-neighbor (J_3) coupling constants.

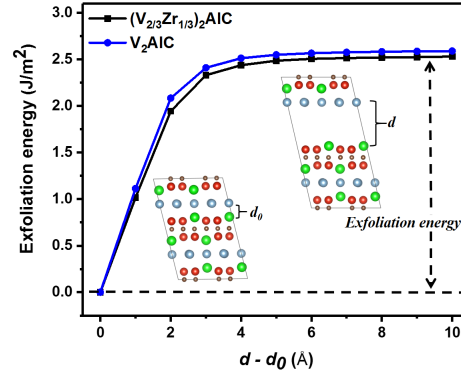


Figure S4: The exfoliation process of $(V_{2/3}Zr_{1/3})_2AlC$ and V_2AlC as a reference

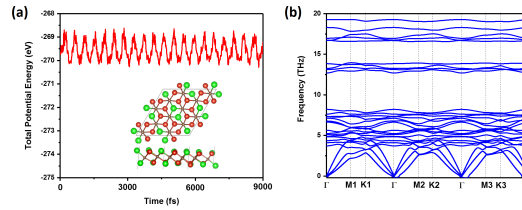


Figure S5: (a) Variations of the total potential energy of $(V_{2/3}Zr_{1/3})_2C$ during ab initio molecular dynamics simulations at 300 K. (b) Phonon dispersion curves for $(V_{2/3}Zr_{1/3})_2C$.

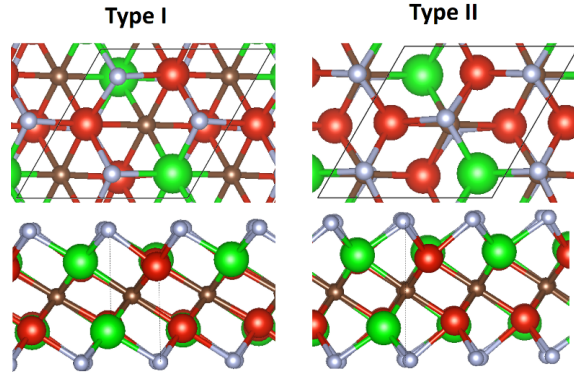


Figure S6: To take $(V_{2/3}Zr_{1/3})_2CF_2$ as an example, two possible types for functional atoms/groups are presented.

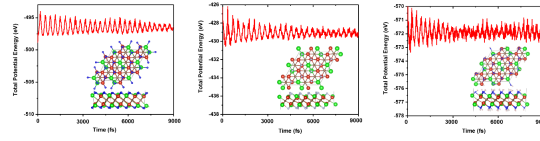


Figure S7: Variations of the total potential energy of $(V_{2/3}Zr_{1/3})_2CT_2$ (T = O, F and OH) during ab initio molecular dynamics simulations at 300 K.

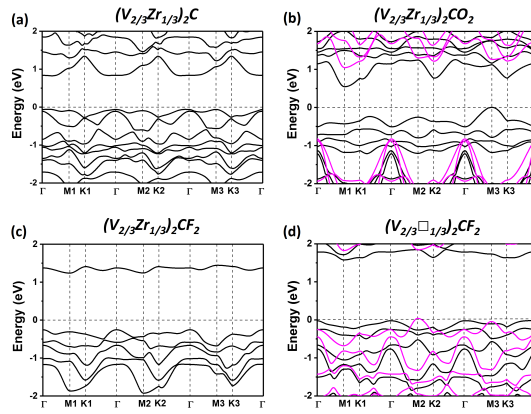


Figure S8: The band structure of $(V_{2/3}Zr_{1/3})_2C$, $(V_{2/3}Zr_{1/3})_2CO_2$, $(V_{2/3}Zr_{1/3})_2CF_2$ and $(V_{2/3}\square_{1/3})_2CF_2$. Black and pink color present spin up and down.

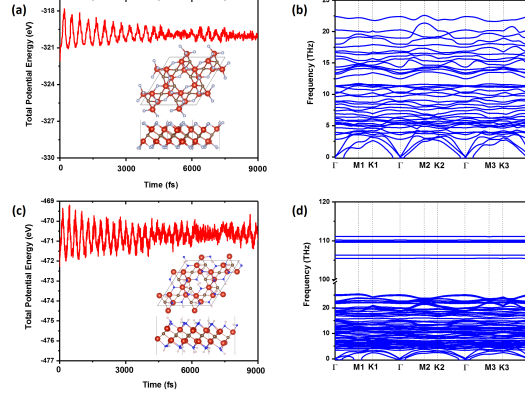


Figure S9: (a) and (c) Variations of the total potential energy of $(V_{2/3}Zr_{1/3})_2CF_2$ and $(V_{2/3}Zr_{1/3})_2C(OH)_2$ during ab initio molecular dynamics simulations at 300 K. (b) and (d) Phonon dispersion curves for $(V_{2/3}Zr_{1/3})_2CF_2$ and $(V_{2/3}Zr_{1/3})_2C(OH)_2$.

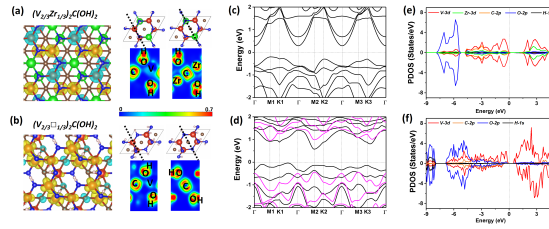


Figure S10: (a) and (b) The inserted background figure shows spin polarized charge densities on $(V_{2/3}Zr_{1/3})_2C(OH)_2$ and $(V_{2/3}\square_{1/3})_2C(OH)_2$, where spin up and spin down densities are shown in yellow and light blue color, respectively. The slices (dot lines) of electron localization function (ELF) maps are perpendicular to (001) direction. (c) and (d) The band structure of $(V_{2/3}Zr_{1/3})_2C(OH)_2$ and $(V_{2/3}\square_{1/3})_2C(OH)_2$. Black and pink color present spin up and down. (e) and (f) The project density of states (PDOS) of $(V_{2/3}Zr_{1/3})_2CF_2$ and $(V_{2/3}Zr_{1/3})_2C(OH)_2$. Fermi level is set up to zero with the black dot line.

3 Tables

<i>Configurations</i>	<i>L</i>	<i>d₁</i>	<i>d₂</i>	<i>d₃</i>	<i>Q(V)</i>	<i>Q(Zr)</i>	<i>Q(C)</i>	<i>Q(O)</i>	<i>Q(F)</i>
V ₂ C	5.435	2.111	2.111	/	-1.33	/	2.65	/	/
(V _{2/3} Zr _{1/3}) ₂ C	5.368	2.127	2.099	2.223	-1.17	-1.33	2.40	/	/
(V _{2/3} Zr _{1/3}) ₂ CO ₂	5.262	2.087	2.084	2.429	-2.12	-2.32	1.96	1.21	/
(V _{2/3} Zr _{1/3}) ₂ CF ₂	5.485	2.109	2.226	2.256	-1.81	-2.14	2.18	/	0.81
(V _{2/3} Zr _{1/3}) ₂ C(OH) ₂	5.508	2.225	2.225	2.171	-1.81	-2.09	2.24	1.80	/
(V _{2/3} □ _{1/3}) ₂ CF ₂	5.136	2.032	2.107	/	-2.21	/	1.59	/	0.70
(V _{2/3} □ _{1/3}) ₂ C(OH) ₂	5.157	1.938	2.042	/	-2.19	/	1.64	1.63	/

Table S1: Calculated structural characteristics of V₂C MXene, pristine (V_{2/3}Zr_{1/3})₂C MXene, three different (V_{2/3}Zr_{1/3})₂CX₂ MXenes and two ordered divacancy (V_{2/3}□_{1/3})₂CX₂ MXene. *L* is the lattice constant. *d₁* and *d₂* are bond lengths of V-C, *d₃* is bond length of Zr-C. *Q* is amount of carried charges by Bader charge analysis.

	ΔE_{CBM} (eV)	ΔE_{VBM} (eV)	<i>Band gap</i> <i>Up</i> (eV)	<i>Band gap</i> <i>Down</i> (eV)	ΔE (meV)	J_1 (meV)	J_2 (meV)	J_3 (meV)	<i>T_c</i> (K)	<i>M</i> (μB)
(V _{2/3} Zr _{1/3}) ₂ CO ₂	0.47	-1.12	0.53	1.85	33.59	76.78	23.02	43.68	300	4
(V _{2/3} □ _{1/3}) ₂ CF ₂	0.24	0.02	1.55	1.83	22.93	8.11	8.16	14.76	30	2
(V _{2/3} □ _{1/3}) ₂ C(OH) ₂	0.37	-0.40	0.61	1.39	2.53	1.30	3.76	-1.23	10	2

Table S2: The characteristic parameter (ΔE_{CBM} , ΔE_{VBM} and band gaps) in unit of eV of energy bands of related MXenes by performed HSE06 calculations. ΔE is the magnetic exchange energy (in meV). *T_c* is the Curie temperature (in K). *M* is the magnetization per unit cell (in μB).